SNUTP 99–026
May 1999

Polarization effects on W boson pair productions with the extra neutral gauge boson at the e^+e^- Linear Collider

Dong-Won Jung[a*], Kang Young Lee[b†], H. S. Song[a,b‡], and Chaehyun Yu[a§]

Department of Physics, Seoul National University, Seoul 151–742, Korea

Center for Theoretical Physics, Seoul National University, Seoul 151–742, Korea

Abstract

We perform the comprehensive analysis of the polarization effects on the $e^+e^- \to W^+W^-$process in the presence of the extra neutral gauge boson at the LC energies. Consideration of the polarizations of the produced W bosons and the beam polarizations provides substantial enhancements of the sensitivity to the Z–Z' mixing angles in various models and the asymmetry variables also give the strict constraints on the mixing angles. We find that the χ–model and the left-right model get the strict constraint from σ_{LL}^{unpol} while the ψ–model and the η–model from the beam polarization asymmetry.

Typeset using REVTEX

*dwjung@zoo.snu.ac.kr

†kylee@ctp.snu.ac.kr

‡hssong@physs.snu.ac.kr

§chyu@zoo.snu.ac.kr

I. INTRODUCTION

Pair production of W bosons is one of the principal process to study the electroweak gauge symmetry in the future e^+e^- linear colliders (LC). The cross section for $e^+e^- \to W^+W^-$ and its angular distribution depend upon various properties of the W boson such as mass, decay widths etc.. This process is also sensitive to the triple gauge boson couplings (TGC) of the $WW\gamma$ and WWZ vertices which enable us to study the nonabelian nature of the gauge structure for the electroweak theory of the Standard Model (SM). These analyses can be carried out at the LC energies ($\sqrt{s} \geq 500$ GeV), promising sensitivities of order 1 % and expected better [1].

Polarizations of the electron and positron beams provide very effective tools to investigate the new physics effects, particularly useful for the $e^+e^- \to W^+W^-$process. Using the right-handed polarized electron beam, the t-channel neutrino exchange diagram of the SM depicted in Fig. 1 (a) is switched off, which occupies a large fraction of the events. The absence of the SM t-channel contribution results in the sensitivity to the existence of remaining new physics effects in the charged current sector and the relative enhancements of them in the neutral current interactions by the great reduction of the SM background. Furthermore each helicity channel shows peculiar behavior depending upon the beam polarizations. Therefore it would be fruitful in search of the new physics beyond the SM to consider the polarization observables together with beam polarizations at this process.

In many scenarios that the gauge symmetries of the SM are extended by adding extra symmetries or embedded into a larger gauge group, we have one or more new heavy neutral gauge bosons. The recent bounds of the new gauge boson masses come from the direct search at $p\bar{p}$ collider via Drell–Yan production and subsequent decay to charged leptons [2] while indirect constraints for the Z' mass and mixing angles are given from high precision LEP data at Z peak energy and various low energy neutral current experiment data [3–8]. In the present work, we consider

$$e^-(k_1, \kappa) + e^+(k_2, -\kappa) \to W^-(p_1, \lambda_1) + W^+(p_2, \lambda_2) \tag{1}$$

with an Z' boson involved in SO(10) and string inspired E_6 grand unified theories (GUTs), which are theoretically well–motivated and have been extensively studied in both theoretical and experimental fields [9,10]. Here, k_i and p_i denote the particle momenta while κ and λ the helicities. Incorporating the extra neutral gauge boson, deviations of the TGCs from the SM predictions would be also introduced as well as the corrections to the neutral current interactions. Identifying the final states as ordinary W bosons, the TGCs come from the $W_1W_2W_3$ term out of the $SU(2)_L$ gauge kinetic terms in the gauge eigenstates and this term leads to an additional $\xi\ WWZ'$ term as well as the ordinary $WW\gamma$ and WWZ couplings in the presence of the Z' boson. We note that the additional WWZ' term always accompanies the Z–Z' mixing angle ξ. Thus the Z' exchange diagram depicted in Fig. 1 (b) is doubly suppressed by the mixing angle ξ and the inverse square of the Z' mass, both of which are expected to be the same order of magnitudes away from the Z' peak. Hence the $e^+e^- \to W^+W^-$process with the Z' boson depends only on ξ keeping the leading corrections of the Z' boson effects off the Z' resonance. It is favorable to set the bounds on the mixing angle ξ from this process with less contaminations of other model–dependent parameters while the $e^+e^- \to f\bar{f}$ processes depend on both the mixing angle ξ and the mass of the Z' boson at the LC.

In this paper, we present the comprehensive analysis of the polarization effects on the W pair production at the e^+e^- collider with an Z' boson at $\sqrt{s} = 500$ GeV and 1 TeV, which are typical center-of-mass (CM) energies of the LC [1]. Similar analyses on this topic have been done previously in the case that the Z' mass is about a few hundred GeV [11,12], that the incident beams are polarized [13], and that one focuses on the backward direction enhancements [14]. Our analysis is performed with the polarized cross sections of the produced W pair and the asymmetry variables with or without beam polarizations. We assume that the mass of the Z' boson is quite large and the Z' effects contribute to the process through only the mixing angle ξ. This paper is organized as follows. In Section II, we briefly review the models involving the additional Z' bosons: the extra

U(1) symmetries and the left-right (LR) model. We calculate the helicity amplitudes and discuss the possible enhancements of the Z' effects for the polarized cross sections in Section III. More analyses on the asymmetry variables are given in Section IV. Finally we conclude in Section V.

II. THE MODELS

When the unifying gauge group breaks to its subgroups, extra U(1) often appears in many GUT models as an intermediate stage involving an additional neutral gauge boson. Here we consider the χ, ψ and η models which occur in the symmetry breaking of SO(10) or string inspired E_6 GUTs according to the path of the gauge symmetry breaking pattern: $SO(10) \to SU(5)\times U(1)_\chi$, $E_6 \to SO(10)\times U(1)_\psi$, $E_6 \to$ rank 5 groups, respectively. In the latter case, the corresponding Z'_η boson is given by a linear combination of the Z'_χ and Z'_ψ such that $Z'_\eta = \sqrt{3/8}Z'_\chi - \sqrt{5/8}Z'_\psi$. The LR model based on the $SU(2)_L\times SU(2)_R\times U(1)$ gauge group is also considered, which is another subgroup of SO(10).

In the presence of extra neutral gauge bosons, the relevant terms of the most general lagrangian is given by

$$\mathcal{L} = \mathcal{L}_m + \mathcal{L}_{NC} + \mathcal{L}_{CC}, \tag{2}$$

where

$$\begin{aligned}
\mathcal{L}_m &= \frac{1}{2}m^2_{Z_1}Z_{1\mu}Z_1^\mu + \frac{1}{2}m^2_{Z_2}Z_{2\mu}Z_2^\mu + \delta m^2 Z_{1\mu}Z_2^\mu, \\
\mathcal{L}_{NC} &= -\frac{1}{2}g_1\sum_f \bar{f}\gamma_\mu(g^f_{0V} - g^f_{0A}\gamma_5)fZ_1^\mu - \frac{1}{2}g_2\sum_f \bar{f}\gamma_\mu(h^f_{0V} - h^f_{0A}\gamma_5)fZ_2^\mu.
\end{aligned} \tag{3}$$

In the case of an additional U(1), the charged current interaction term $\mathcal{L}_{CC}$ is same as that of the SM. The model parameter h^f_{0V} and h^f_{0A} are listed in the Table I and the coupling constant of the Z_2 boson is given by

$$g_2 = \sqrt{\frac{5}{3}}\, g_1 \sin\theta_W \sqrt{\lambda_g}, \tag{4}$$

where λ_g depends on the symmetry breaking pattern and of $\mathcal{O}(1)$ [9]. We let $\lambda_g = 1$ assuming that the gauge group breaks directly to $\mathrm{SU}(3)_C \times \mathrm{SU}(2)_L \times \mathrm{U}(1)_Y$.

	χ model	ψ model	η model
h_{V0}	$2/\sqrt{10}$	0	$3/2\sqrt{15}$
h_{A0}	$1/\sqrt{10}$	$1/\sqrt{6}$	$-1/2\sqrt{15}$

Table 1. *The vector and axial-vector couplings of charged leptons to the Z' gauge boson in the SO(10) and E_6 GUT models.*

After diagonalizing the mass matrix, we define the mass eigenstates of neutral gauge bosons as

$$\begin{pmatrix} Z_1 \\ Z_2 \end{pmatrix} = \begin{pmatrix} \cos\xi & -\sin\xi \\ \sin\xi & \cos\xi \end{pmatrix} \begin{pmatrix} Z \\ Z' \end{pmatrix}, \tag{5}$$

where the mixing angle ξ is given by

$$\tan 2\xi = -\frac{2\delta m^2}{m_{Z_2}^2 - m_{Z_1}^2}. \tag{6}$$

In terms of Z and Z' states, the neutral current interaction terms are written as

$$\mathcal{L}_{NC} = -\frac{1}{2} g_1 \sum_f \bar{f}\gamma_\mu (g_V^f - g_A^f \gamma_5) f Z^\mu - \frac{1}{2} g_2 \sum_f \bar{f}\gamma_\mu (h_V^f - h_A^f \gamma_5) f Z'^\mu, \tag{7}$$

with the vector and axial-vector couplings

$$g_{V,A}^f = g_{0V,A}^f + \xi\ h_{0V,A}^f \frac{g_2}{g_1}, \quad h_{V,A}^f = h_{0V,A}^f - \xi\ g_{0V,A}^f \frac{g_1}{g_2}, \tag{8}$$

by keeping the leading order in ξ. Since there are no corrections to the charged current sector in this case, the new physics effects reside in the mixing angle ξ only.

In the case of the LR model, one can find the detailed review of the LR model lagrangian in Ref. [8,10] and references therein. Here, we follow the formulae of Ref. [8]. The mass

matrix of neutral gauge bosons $(B_\mu, W^L_{3\mu}, W^R_{3\mu})$ is diagonalised by 3 angles θ_W, θ_R, and ξ to obtain the physical eigenstates (A_μ, Z_μ, Z'_μ). Among these angles, θ_W is corresponding to the Weinberg angle of the SM which describes the A–Z_1 mixing while ξ is the Z–Z' mixing angle corresponding to Eq. (6). Meanwhile θ_R is an additional parameter depending upon the model. It is preferred to write the lagrangian in terms of the left–right basis instead of the form of Eq. (3). After the diagonalization, we write the neutral current sector

$$\begin{aligned}
\mathcal{L}_{\rm NC} = & -e\overline{f}\not{A}\Big[(T_{L3}+S)P_L + (T_{R3}+S)P_R\Big]f \\
& -\overline{f}\not{Z}\Big[\Big(g_L c_W c_\xi T_{L3} - g_1(c_R s_W c_\xi + s_R s_\xi)S\Big)P_L \\
& \quad +\Big(g_R(c_R s_\xi - s_R s_W c_\xi)T_{R3} - g_1(c_R s_W c_\xi + s_R s_\xi)S\Big)P_R\Big]f \\
& -\overline{f}\not{Z}'\Big[\Big(-g_L c_W s_\xi T_{L3} + g_1(c_R s_W s_\xi - s_R c_\xi)S\Big)P_L \\
& \quad +\Big(g_R(c_R c_\xi + s_R s_W s_\xi)T_{R3} + g_1(c_R s_W s_\xi - s_R c_\xi)S\Big)P_R\Big]f, \qquad (9)
\end{aligned}$$

where $c_i = \cos\theta_i$, $s_i = \sin\theta_i$ and $c_\xi = \cos\xi$, $s_\xi = \sin\xi$. Here g_L is the gauge coupling constant of $\mathrm{SU}(2)_L$ group, g_R is that of $\mathrm{SU}(2)_R$, g_1 is that of $\mathrm{U}(1)$ and S is the $\mathrm{U}(1)$ charge. Since we consider the general case of the model, g_L need not be same as g_R. Looking at the couplings to the photon, we define the electric charge $Q = T_{L3} + T_{R3} + S$ and obtain the relations among the couplings:

$$e = g_L s_W = g_R s_R c_W = g_1 c_R c_W. \qquad (10)$$

The neutral current coupled to the Z boson up to the leading order in ξ is given by

$$J^\mu_Z = \frac{e}{s_W c_W}\overline{f}\gamma^\mu\Big[T_{L3} - s^2_W Q + \xi s_W\Big(t_R(T_{L3}-Q) + (t_R + \frac{1}{t_R})T_{R3}\Big)\Big]f, \qquad (11)$$

where $t_R = s_R/c_R$.

In the LR model, there is also a mixing in the charged current sector which affects the t–channel diagram. However if we fix the final states as the ordinary W boson pair, both of the charged current interactions should be right-handed and the exchanged neutrino is also the right-handed one. As a result, the correction to the t–channel diagram is suppressed by the quadratic factor of the W boson mixing angle and the inverse of the

heavy right-handed neutrino mass even in the leading order of corrections. It is natural to regard the mixing angle of the charged current sector as the same order of magnitude of that of the neutral current sector. Hence we can safely neglect the corrections of the LR model to the t–channel when keeping the leading corrections of extra gauge boson effects. We conclude that we can concentrate on the correction to the Ze^+e^- vertex for the Z' boson effects even in the LR model.

III. W BOSON PAIR PRODUCTION

The W pair is produced through the s–channel diagrams mediated by neutral gauge bosons and the t–channel mediated by neutrino shown in Fig.1. Denoting the helicity of the electron by $\kappa = \pm 1$ and the helicities of the W^- and W^+ bosons by λ_1 and λ_2, respectively as in the Eq. (1), the helicity amplitudes are given by

$$\mathcal{M}^{\kappa}_{SM}(\lambda_1,\lambda_2) = \frac{e^2}{2\sin^2\theta_W}\frac{1}{t}\mathcal{M}^{\kappa}_1\delta_{\kappa-} + e^2\Big(\frac{1}{s} - \frac{\epsilon_\kappa}{\sin^2\theta_W}\frac{1}{s-m_Z^2}\Big)(2\mathcal{M}^{\kappa}_3 - \mathcal{M}^{\kappa}_2), \tag{12}$$

where the Ze^+e^- coupling is

$$\epsilon_\kappa = -\frac{1}{2}\delta_{\kappa-} + \sin^2\theta_W. \tag{13}$$

The $\mathcal{M}^{\kappa}_i$ are given by

$$\begin{aligned}
\mathcal{M}^{\kappa}_1 &= \overline{v}(p_2)\not{\epsilon}^*_2(\not{k}_2 - \not{p}_2)\not{\epsilon}^*_1\omega_\kappa u(p_1),\\
\mathcal{M}^{\kappa}_2 &= \overline{v}(p_2)(\not{k}_2 - \not{k}_1)(\epsilon^*_1\cdot\epsilon^*_2)\omega_\kappa u(p_1),\\
\mathcal{M}^{\kappa}_3 &= \overline{v}(p_2)[\not{\epsilon}^*_2(\epsilon^*_1\cdot k_2) - \not{\epsilon}^*_1(\epsilon^*_2\cdot k_1)]\omega_\kappa u(p_1),
\end{aligned} \tag{14}$$

where ω_κ is the helicity projection operator and ϵ^*_1 (ϵ^*_2) is a polarization vector of $W^-(W^+)$.

Keeping only the leading corrections in ξ, the scattering amplitude is written as

$$\begin{aligned}
\mathcal{M}^{\kappa}(\lambda_1,\lambda_2) &= \mathcal{M}^{\kappa}_{SM}(\lambda_1,\lambda_2) + \xi\mathcal{M}^{\kappa}_{NP}(\lambda_1,\lambda_2),\\
\mathcal{M}^{\kappa}_{NP}(\lambda_1,\lambda_2) &= \frac{e^2}{\sin^2\theta_W}\frac{1}{s-m_Z^2}(h^e_{0V} - \kappa h^e_{0A})(2\mathcal{M}^{\kappa}_3 - \mathcal{M}^{\kappa}_2),
\end{aligned} \tag{15}$$

where h^e_{0V} and h^e_{0A} are model-dependent parameters given in the previous section. Hereafter we drop the superscript e.

In the CM frame, the helicity amplitudes are given by

$$\begin{aligned}
\mathcal{M}^-(+,+) &= e^2 \sin\theta \left[\frac{1}{\sin^2\theta_W}\frac{s}{4t}(\cos\theta-\beta)-\alpha_L\beta\right],\\
\mathcal{M}^-(+,0) &= e^2\frac{\sqrt{2}}{\sqrt{1-\beta^2}}(\cos\theta+1)\left[\frac{1}{2\sin^2\theta_W}\frac{s}{4t}(2\beta+1-2\cos\theta-\beta^2)+\alpha_L\beta\right],\\
\mathcal{M}^-(+,-) &= e^2\sin\theta(\cos\theta+1)\frac{1}{\sin^2\theta_W}\frac{s}{4t},\\
\mathcal{M}^-(0,+) &= e^2\frac{\sqrt{2}}{\sqrt{1-\beta^2}}(\cos\theta-1)\left[\frac{1}{2\sin^2\theta_W}\frac{s}{4t}(2\beta-1-2\cos\theta+\beta^2)+\alpha_L\beta\right],\\
\mathcal{M}^-(0,0) &= e^2\frac{1}{1-\beta^2}\sin\theta\left[\frac{1}{4\sin^2\theta_W}\frac{s}{4t}(3\beta-2\cos\theta-\beta^3)+\alpha_L\beta(3-\beta)\right],\\
\mathcal{M}^-(-,+) &= e^2\sin\theta(\cos\theta-1)\frac{1}{\sin^2\theta_W}\frac{s}{4t},
\end{aligned} \tag{16}$$

and

$$\begin{aligned}
\mathcal{M}^+(+,+) &= e^2\alpha_R\beta\sin\theta,\\
\mathcal{M}^+(+,0) &= e^2\frac{\sqrt{2}}{\sqrt{1-\beta^2}}\alpha_R\beta\sin\theta(\cos\theta-1),\\
\mathcal{M}^+(+,-) &= 0,\\
\mathcal{M}^+(0,+) &= e^2\frac{\sqrt{2}}{\sqrt{1-\beta^2}}\alpha_R\beta\sin\theta(\cos\theta+1),\\
\mathcal{M}^+(0,0) &= e^2\frac{1}{1-\beta^2}\alpha_R\beta\sin\theta(3-\beta^2),\\
\mathcal{M}^+(-,+) &= 0,
\end{aligned} \tag{17}$$

where $\beta=\sqrt{1-4m_W^2/s}$, *theta* is the scattering angle and

$$\begin{aligned}
\alpha_L &= \left(1-\frac{s}{s-m_Z^2}\frac{1}{2\sin^2\theta_W}(g_V+g_A)\right),\\
\alpha_R &= \left(1-\frac{s}{s-m_Z^2}\frac{1}{2\sin^2\theta_W}(g_V-g_A)\right),
\end{aligned} \tag{18}$$

with g_V and g_A given in Eq. (8). The CP invariance leads to

$$\mathcal{M}^\kappa(0,\pm)=\mathcal{M}^\kappa(\mp,0),\qquad \mathcal{M}^\kappa(+,+)=\mathcal{M}^\kappa(-,-). \tag{19}$$

These results agree with the formulae in Ref. [15].

The differential cross section is obtained by the sum of the polarized cross sections

$$\frac{d\sigma_{total}}{d\cos\theta} = \frac{1}{4}\sum_{\lambda_1,\lambda_2}\left[(1+P_-)(1-P_+)\frac{d\sigma^+(\lambda_1,\lambda_2)}{d\cos\theta} + (1-P_-)(1+P_+)\frac{d\sigma^-(\lambda_1,\lambda_2)}{d\cos\theta}\right], \quad (20)$$

where P_- (P_+) is the polarization of the electron (positron) beam and the polarized differential cross sections are given by

$$\frac{d\sigma^\kappa(\lambda_1,\lambda_2)}{d\cos\theta} = \frac{\beta}{32\pi s}|\mathcal{M}^\kappa(\lambda_1,\lambda_2)|^2. \quad (21)$$

In order to estimate the search bound of the Z' contributions, we take the linear approximation of the cross section under the assumption that the mixing angle ξ is very small:

$$\sigma = \sigma_{SM} + \xi\sigma_1. \quad (22)$$

We plot the ratio of the correction term σ_1 to the SM cross section σ_{SM} with varying the CM energy $\sqrt{s}$ in Fig. 2 and 3, when the electron beam is unpolarized and right-handed polarized respectively. When the unpolarized electron beam is used, the large neutrino exchange t–channel contribution conceals the new physics effects. Considering the cross section of both longitudinally polarized W boson pair, however, we find that $|\sigma_1^{LL}/\sigma_{SM}^{LL}|$ increases according to the increase of $\sqrt{s}$ in the Fig. 2, which implies that the observable σ_{LL} becomes sensitive to the Z' corrections at high energy collisions. In the limit of $\sqrt{s} \gg m_z$, the leading term of the SM helicity amplitude of both longitudinally polarized W pair, $\mathcal{M}_{SM}^\kappa(0,0)$ is of order of m_z^2/s while that of $\mathcal{M}_{NP}^\kappa(0,0)$ is of order 1. As a result, the ratio is given by

$$\left|\frac{\sigma_1^{LL}}{\sigma_{SM}^{LL}}\right| \sim \frac{\mathcal{M}_{SM}(0,0)\mathcal{M}_{NP}(0,0)}{\mathcal{M}_{SM}(0,0)^2} \propto \frac{s}{m_z^2}, \quad (23)$$

which rapidly increases along with the CM energy and results in the sensitivity to the Z' effects. We expect to probe the mixing angle ξ more precisely from the observable σ^{LL} than from the total cross section.

Even though the polarized cross section σ^{LL} is sensitive to the mixing angle ξ, we should put up with a statistical loss because σ^{LL} is much smaller than σ_{tot}. Alternatively

we suggest to use the right-handed electron beam which avoids masking the large t–channel contribution and also show the remarkable feature like Eq. (23). All of the SM helicity amplitudes for right-handed electron beam, $\mathcal{M}^{+}_{SM}$, are proportional to the factor

$$\frac{1}{s} - \frac{1}{s - m_Z^2} = -\frac{m_Z^2}{s} \cdot \frac{1}{s - m_Z^2}, \tag{24}$$

while $\mathcal{M}^{+}_{NP}$ are proportional to $1/(s - m_Z^2)$ with the common part of the helicity amplitudes $(2\mathcal{M}^{+}_{3} - \mathcal{M}^{+}_{2})$ in the Eq. (15). Accordingly all ratios of helicity cross sections $|\sigma_1/\sigma_{SM}|$ are always proportional to s/m_Z^2 as shown in the Fig. 3. Thus the sensitivity to the new physics effects is yielded even for the total cross section if we use the right-handed electron beam. Moreover it would be statistically favorable to use the total cross section with the right-handed polarized electron beam than to use σ_{LL} with unpolarized beam.

	σ_{LL}^{unpol}		$\sigma_{tot}^{90\%R}$	
	$\sqrt{s}$ =500 GeV	1 TeV	500 GeV	1 TeV
χ	−0.00139	−0.00034	−0.00604	−0.00175
	0.00135	0.00033	0.00557	0.00159
ψ	−0.00782	−0.00186	−0.00654	−0.00184
	0.00635	0.00154	0.00753	0.00216
η	−0.00306	−0.00076	−0.00479	−0.00138
	0.00295	0.00074	0.00437	0.00124
LR	−0.00111	−0.00027	−0.00373	−0.00108
	0.00108	0.00027	0.00345	0.00098

Table 2. *The reaches of the bounds of the mixing angle ξ from the cross section for the both longitudinally polarized W pair with unpolarized e^- beam and the total cross section with 90% right-handed polarized e^- beam. The angular cut $|\cos\theta| < 0.9$ is applied.*

Considering the statistical error and 1% systematic error, the expected bounds of the mixing angle ξ are derived from the polarization observables discussed above at 95% C.L. with the angular cut $|\cos\theta| < 0.9$ and presented in Table II. The integrated luminosities are taken to be as $\int \mathcal{L} = 50$ fb^{-1} for $\sqrt{s} = 500$ GeV and $\int \mathcal{L} = 200$ fb^{-1} for $\sqrt{s} = 1$ TeV [1]. Note that the generation of 100% polarization of the electron beam is hardly reached in practice. We consider the expected polarization of the e^- beam as 90% here. In this case, it still makes a contamination from the neutrino exchange t–channel of the SM contribution, especially in the forward scattering region. The angular cut may reduce the contamination from the t–channel, which should be introduced by the practical reason of the detector geometry. We find that more strict bounds on ξ are derived from σ_{LL}^{unpol} in most cases. For the illustrative purpose we plot the σ_{LL}^{unpol} and $\sigma_{tot}^{90\%R}$ with respect to the mixing angle ξ in the Fig. 4 and 5.

IV. ASYMMETRIES

Parity violation of the electroweak theory is implied by the asymmetry between the left and right couplings of the weak neutral current interaction. The asymmetry variables are essential touchstones to explore the gauge structure of the SM. Labelling the cross sections of the $e^+e^- \to W^+W^-$process by the direction of $W^\pm$ bosons and the helicity of the incident electron beam, we define the forward-backward asymmetry

$$A_{FB} = \frac{\sigma_F - \sigma_B}{\sigma_F + \sigma_B}, \tag{25}$$

where

$$\sigma_F = \int_0^1 d\cos\theta \frac{d\sigma}{d\cos\theta}, \quad \sigma_B = \int_{-1}^0 d\cos\theta \frac{d\sigma}{d\cos\theta}, \tag{26}$$

and the beam polarization asymmetry

$$A_{pol} = \frac{\sigma_R - \sigma_L}{\sigma_R + \sigma_L}, \tag{27}$$

where $\sigma_{L(R)}$ is the cross section with the left- (right-) handed electron beam.

We show the forward-backward asymmetry for each model in the Fig. 6 with respect to the mixing angle ξ to estimate the bounds of it. The beam polarization asymmetry can be defined by both the differential cross sections and integrated ones. Figure 7 shows the one from the total cross sections with respect to ξ while Fig. 8 shows the asymmetries from the differential cross sections with respect to $\cos\theta$. The dotted and dashed lines in the Fig. 8 is corresponding to the most recent bounds on the mixing angle ξ given in Ref. [5,8]. By means of the same manner in the previous section, we estimate the reaches of the bounds of ξ from the asymmetry variables and present the results in Table III. We consider the 1% systematic and the statistical errors at 95% C.L.. It is to be noted that the lower bound of ξ from the forward-backward asymmetry should not be considered seriously since the higher order corrections in ξ become important as shown in the Fig. 6.

	A_{FB}		A_{pol}	
	$\sqrt{s}$ =500 GeV	1 TeV	500 GeV	1 TeV
χ	−0.00404	−0.00110	−0.00220	−0.00057
	0.00385	0.00104	0.00216	0.00056
ψ	−0.02225	−0.02235	−0.00150	−0.00039
	0.00450	0.00429	0.00154	0.00041
η	−0.00920	−0.00250	−0.00126	−0.00033
	0.00840	0.00226	0.00123	0.00032
LR	−0.00324	−0.00088	−0.00120	−0.00031
	0.00309	0.00083	0.00118	0.00031

Table 3. *The reaches of the bounds of the mixing angle ξ from the forward-backward asymmetry A_{FB} and the beam polarization asymmetry A_{pol}. The angular cut $|\cos\theta| < 0.9$ is applied.*

V. CONCLUDING REMARKS

We study the polarization effects on the $e^+e^- \to W^+W^-$process with an extra neutral gauge boson. Since the corrections proportional to the mixing angle ξ relatively increase compared with the SM predictions in this process as shown in the Fig. 2, we expect to obtain the strict bounds on ξ at the high energy collisions of the e^+e^- linear collider. When the CM energy reach to 1 TeV, we show that the Z–Z' mixing angle could be measured up to the order of 10^{-4}. On the other hand, we could set the bounds on the mixing angle with less contaminations from the other parameter $m_{Z'}$ in this process contrary to the fermion pair productions if we keep the leading order in ξ.

In our analysis, the χ–model and the left-right model are shown to get the most strict constraint from the cross section for the both longitudinally polarized W bosons, σ_{LL}^{unpol} while the ψ–model and the η–model get it from the beam polarization asymmetry A_{pol}. We conclude that the consideration of the polarization effects on W boson pair production enable us to probe the Z–Z' mixing angle more precisely. Meanwhile, if we can improve the beam polarization or reduce the systematic errors, we expect that the total cross section with the right-handed electron beam could provide better results since it has a statistical advantage compared with σ_{LL}^{unpol}.

Acknowledgements

This work is supported in part by the Korean Science and Engineering Foundation (KOSEF) through the SRC program of the Center for Theoretical Physics (CTP) at Seoul National University and in part by the Korea Research Foundation as the program of 1998.

REFERENCES

[1] E. Accomando *et. al.*, DESY 97-100.

[2] F. Abe *et al.*, CDF Collaboration, Phys. Rev. Lett. **79**, 2192 (1997).

[3] G. Altarelli, *et al.*, Mod. Phys. Lett. A **5**, 495 (1990); Phys. Lett. B **263**, 459 (1991).

[4] P. Langacker and M. Luo, Phys. Rev. D **45**, 278 (1992);
P. Langacker, M. Luo and A. Mann, Rev. Mod. Phys., **64**, 87 (1992);
J. Erler and P. Langacker, Eur. Phys. J. C **3**, 90 (1998).

[5] J. Erler and P. Langacker, Report No. UPR-0839-T, hep-ph/9903476.

[6] K. S. Babu, C. Kolda and J. March-Russell, Phys. Rev. D **54**, 4635 (1996); *ibid* D **57**, 6788 (1998).

[7] G.-C. Cho, K. Hagiwara and Y. Umeda, Nucl. Phys. **B531**, 65 (1998);
Y. Umeda, G.-C. Cho and K. Hagiwara, Phys. Rev. D **58**, 115008 (1998).

[8] J. Chay, K. Y. Lee and S.-h. Nam, Report No. SNUTP 98-101, KIAS-P 98020, hep-ph/9809298.

[9] J. L. Hewett and T. G. Rizzo, Phys. Rept. **183** , 193 (1989) and references therein.

[10] R. N. Mohapatra and G. Senjanović, Phys. Rev. Lett. **44**, 91 (1980); Phys. Rev. D **23**, 165 (1981); for reviews, see R. N. Mohapatra, *Unification and Supersymmetry* (Springer, New York, 1986).

[11] R. Najima and S. Wakaizumi, Phys. Lett. B **184**, 410 (1987).

[12] P. Kalyniak and M. K. Sundaresan, Phys. Rev. D **35**, 75 (1987).

[13] P. Comas and A. Méndez, Phys. Lett. B **260**, 211 (1991).

[14] A. A. Pankov and N. Paver, Phys. Lett. B **272**, 425 (1991).

[15] W. Beenakker and A. Denner, Int. J. Mod. Phys. A **9**, 4837 (1994).

Figure Captions

Fig. 1 : Feynman diagrams for the $e^+e^- \to W^+W^-$process.

Fig. 2 : The ratios of the correction terms to the Standard Model predictions, $|\sigma_1/\sigma_{SM}|$ with respect to the CM energy when we use the unpolarized electron beam. The solid lines denote the ratios of total cross sections, the dashed lines the ratios of the cross sections of W pair with one longitudinally polarized but one transversely polarized, and the dotted lines the ratios of the cross sections of both longitudinally polarized W pair.

Fig. 3 : The ratios of the correction terms to the Standard Model predictions, $|\sigma_1/\sigma_{SM}|$ with respect to the CM energy when we use the right-handed electron beam. The solid lines denote the ratios of total cross sections, the dashed lines the ratios of the cross sections of W pair with one longitudinally polarized but one transversely polarized, and the dotted lines the ratios of the cross sections of both longitudinally polarized W pair.

Fig. 4 : The cross sections for the both longitudinally polarized W bosons σ_{LL}^{unpol} with respect to the mixing angle ξ when we use the unpolarized electron beam. The dotted lines denote the cross sections of χ model, the short–dashed lines those of ψ model, the long–dashed lines those of η model, and the dash–dotted lines those of LR model.

Fig. 5 : The total cross sections $\sigma_{total}^{90\%R}$ with respect to the mixing angle ξ when we use the 90% right-handed electron beam. The dotted lines denote the cross sections of χ model, the short–dashed lines those of ψ model, the long–dashed lines those of η model, and the dash–dotted lines those of LR model.

Fig. 6 : The forward-backward asymmetry A_{FB} with respect to the mixing angle ξ. The dotted lines denote the asymmetries of χ model, the short–dashed lines those of ψ model, the long–dashed lines those of η model, and the dash–dotted lines those of LR model.

Fig. 7 : The beam polarization asymmetry A_{pol} with respect to the mixing angle ξ. The dotted lines denote the asymmetries of χ model, the short–dashed lines those of ψ model, the long–dashed lines those of η model, and the dash–dotted lines those of LR model.

Fig. 8 : The beam polarization asymmetry A_{pol} from the differential cross sections with respect to the scattering angle $\cos\theta$. The solid lines denote the Standard Model predictions, while the dashed lines the maximal deviations with the mixing angle bounds given in Ref. [5].

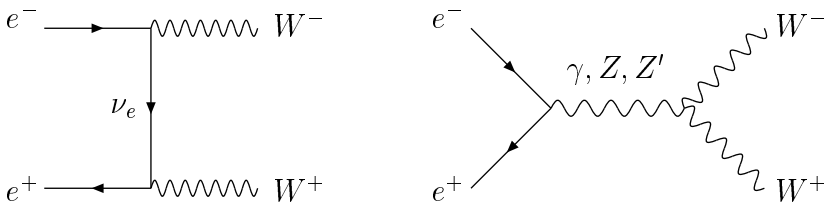

Fig. 1

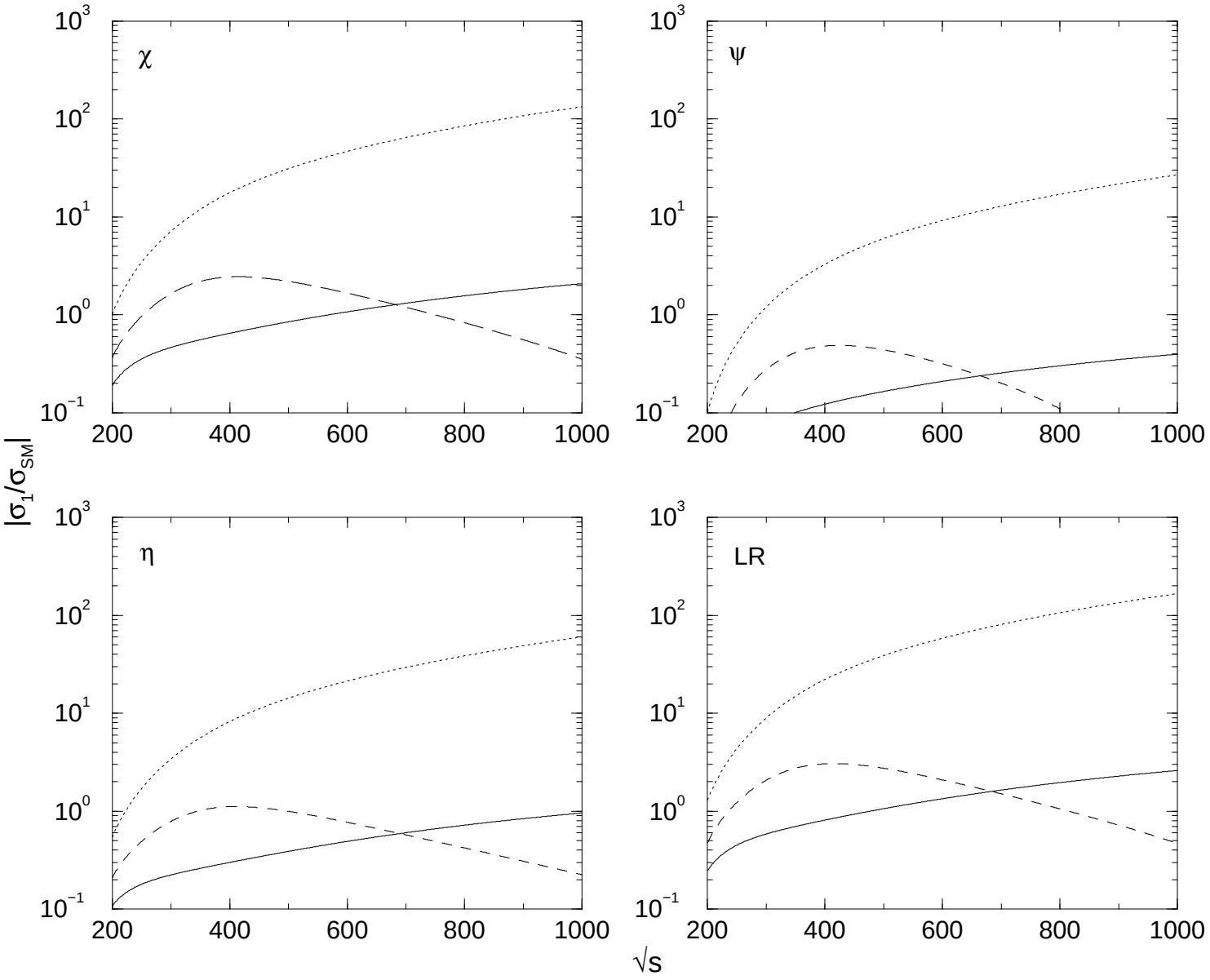
χ
ψ
η
LR
$|\sigma_1/\sigma_{SM}|$
√s
10^3
10^2
10^1
10^0
10^{-1}
200
400
600
800
1000

Fig. 2

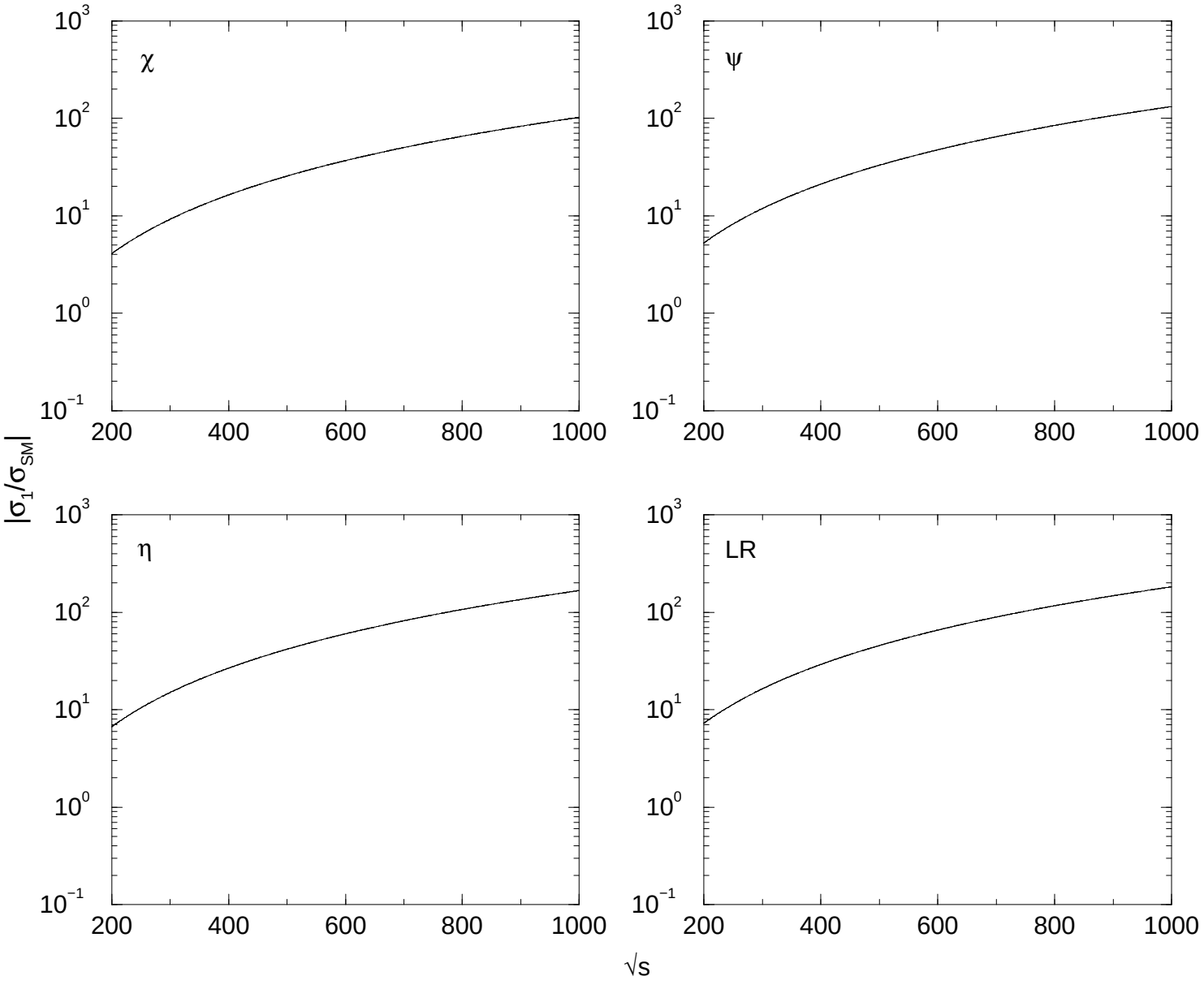
χ
ψ
η
LR
$|\sigma_1/\sigma_{SM}|$
√s
10^3
10^2
10^1
10^0
10^{-1}
200
400
600
800
1000

Fig. 3

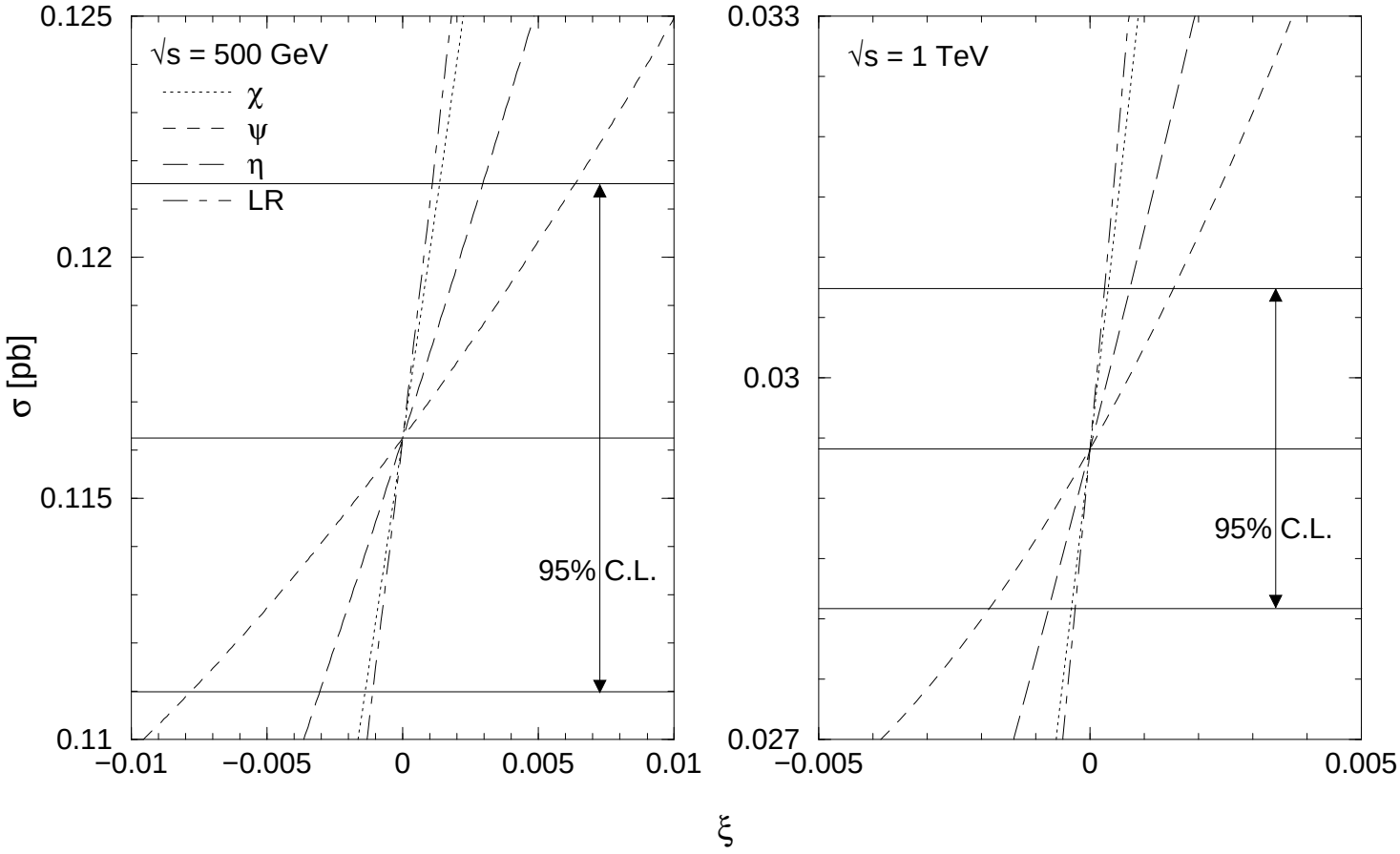
√s = 500 GeV
χ
ψ
η
LR
95% C.L.
σ [pb]
0.125
0.12
0.115
0.11
−0.01
−0.005
0
0.005
0.01
√s = 1 TeV
95% C.L.
0.033
0.03
0.027
−0.005
0
0.005
ξ

Fig. 4

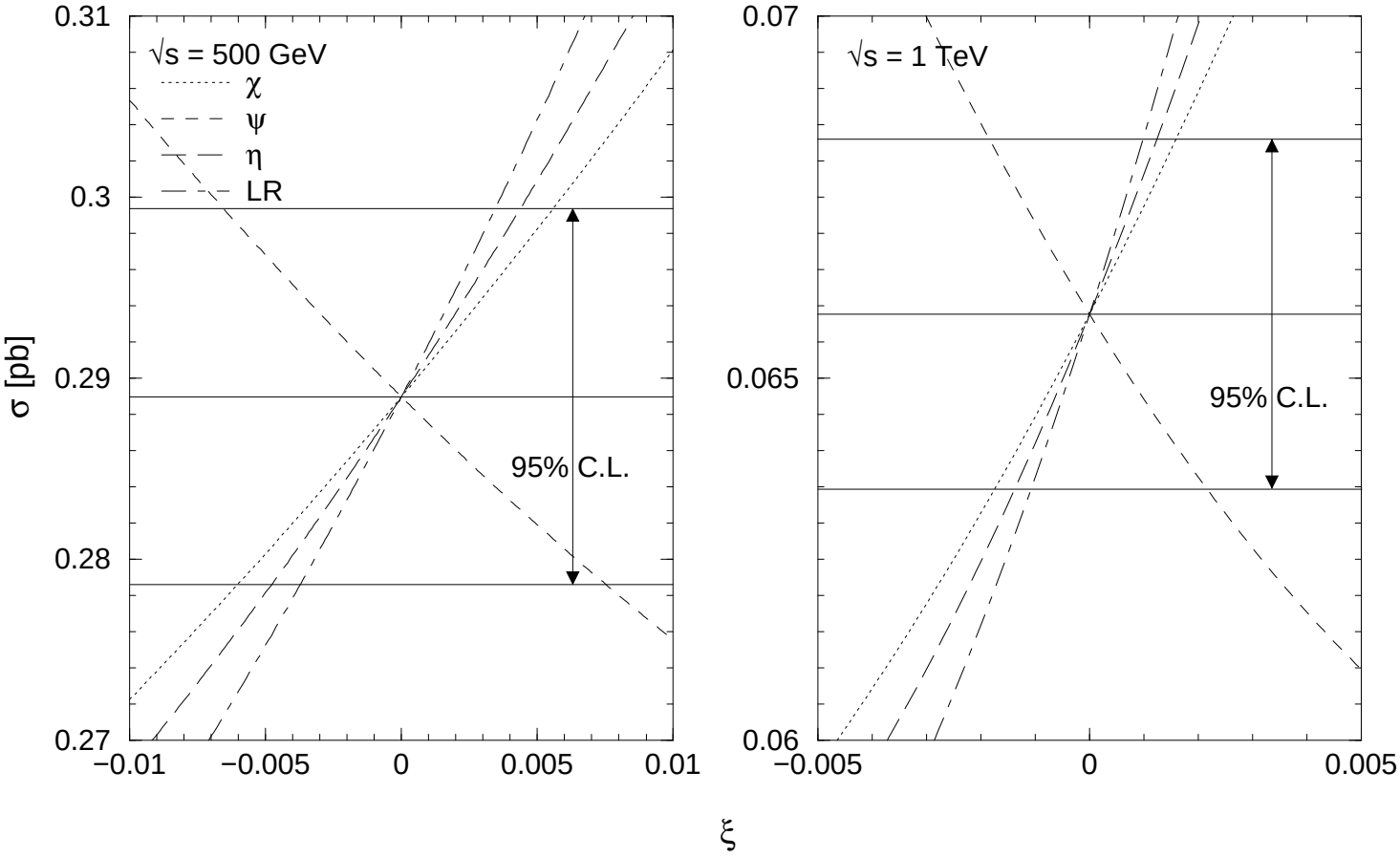
√s = 500 GeV
χ
ψ
η
LR
95% C.L.
σ [pb]
0.31
0.3
0.29
0.28
0.27
−0.01
−0.005
0
0.005
0.01
√s = 1 TeV
95% C.L.
0.07
0.065
0.06
−0.005
0
0.005
ξ

Fig. 5

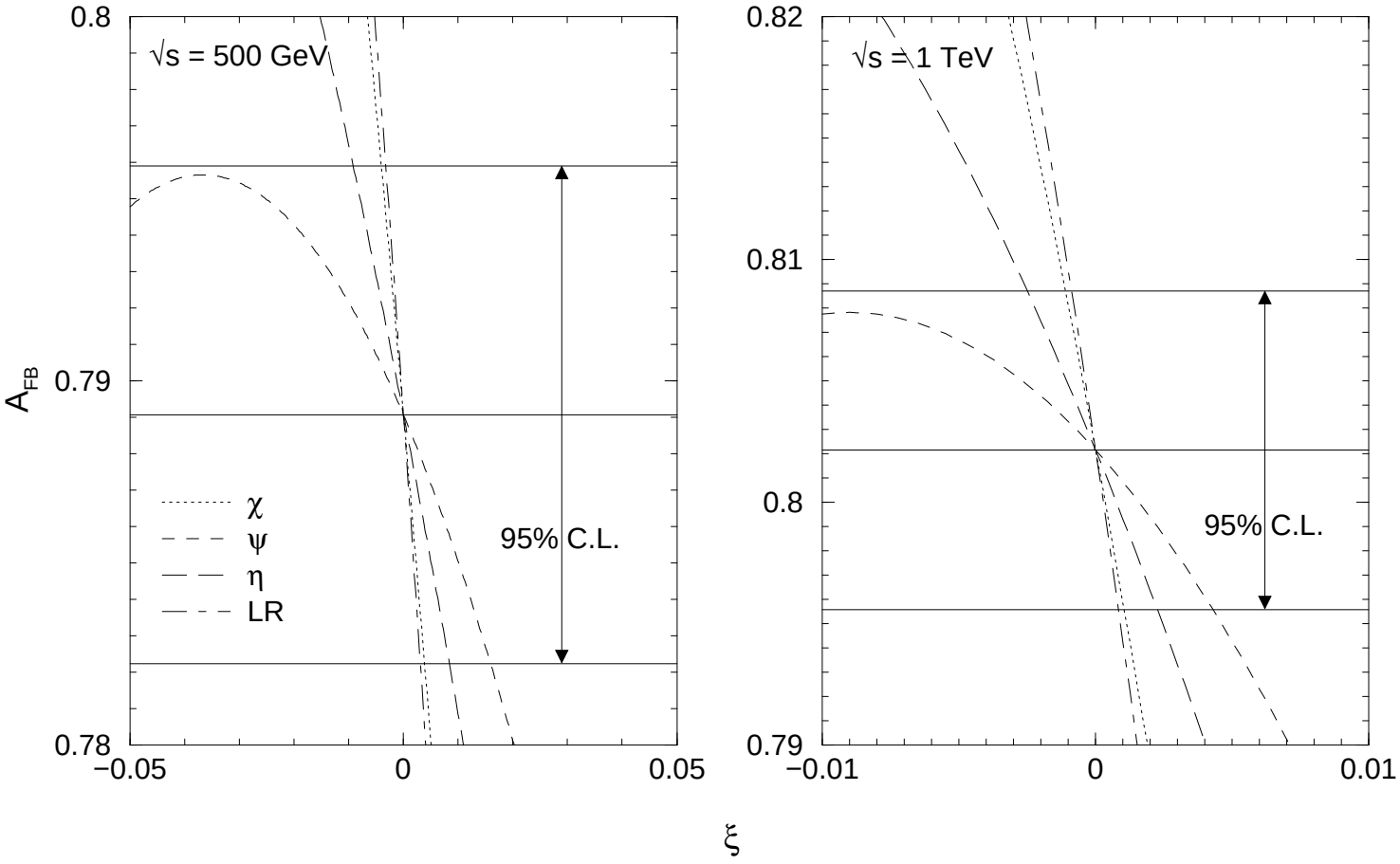
0.8
√s = 500 GeV
0.79
0.78
A_FB
χ
ψ
η
LR
95% C.L.
−0.05
0
0.05
0.82
√s = 1 TeV
0.81
0.8
0.79
95% C.L.
−0.01
0
0.01
ξ

Fig. 6

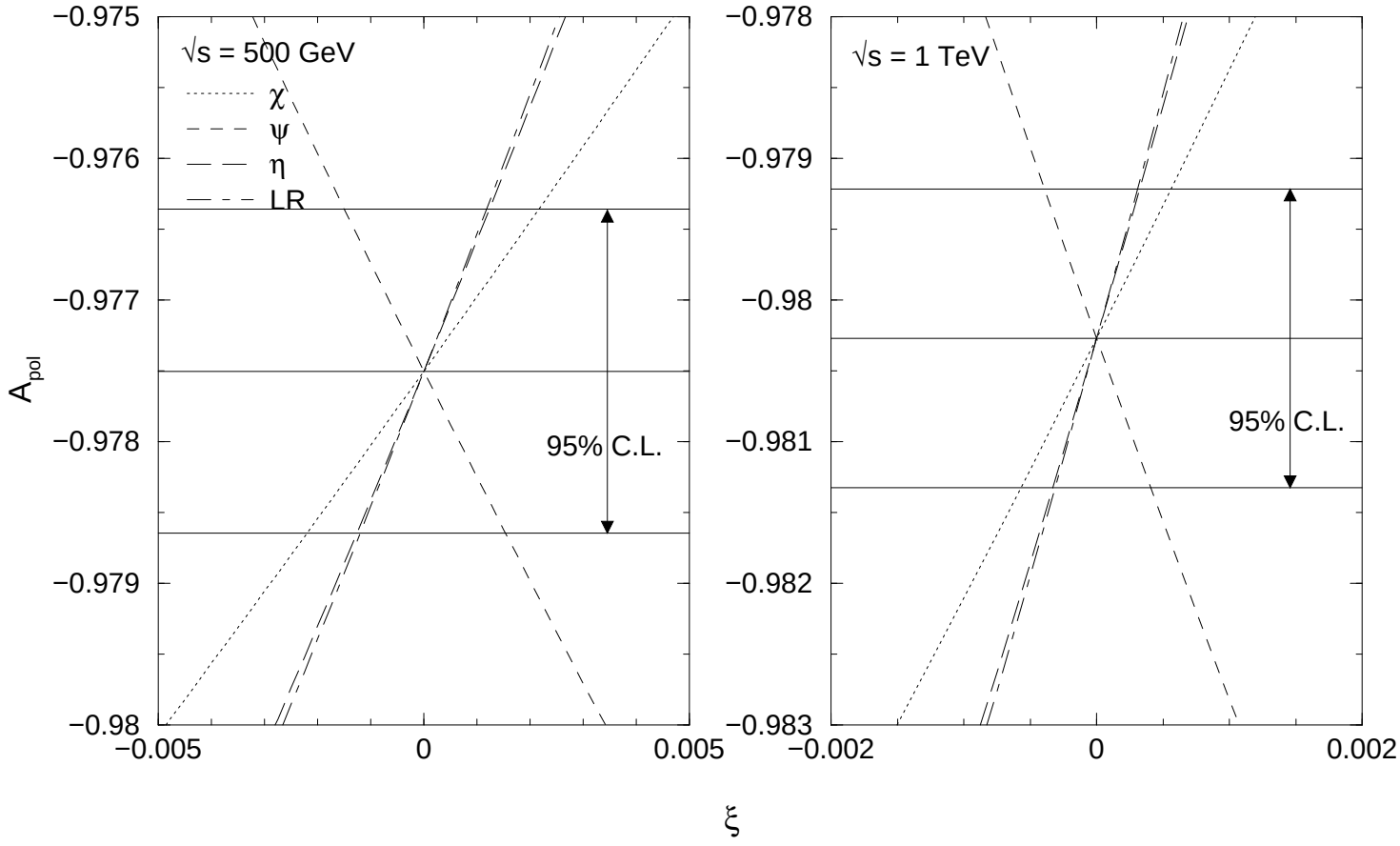
√s = 500 GeV
χ
ψ
η
LR
95% C.L.
√s = 1 TeV
95% C.L.
A_pol
ξ
−0.975
−0.976
−0.977
−0.978
−0.979
−0.98
−0.005
0
0.005
−0.978
−0.979
−0.98
−0.981
−0.982
−0.983
−0.002
0
0.002

Fig. 7

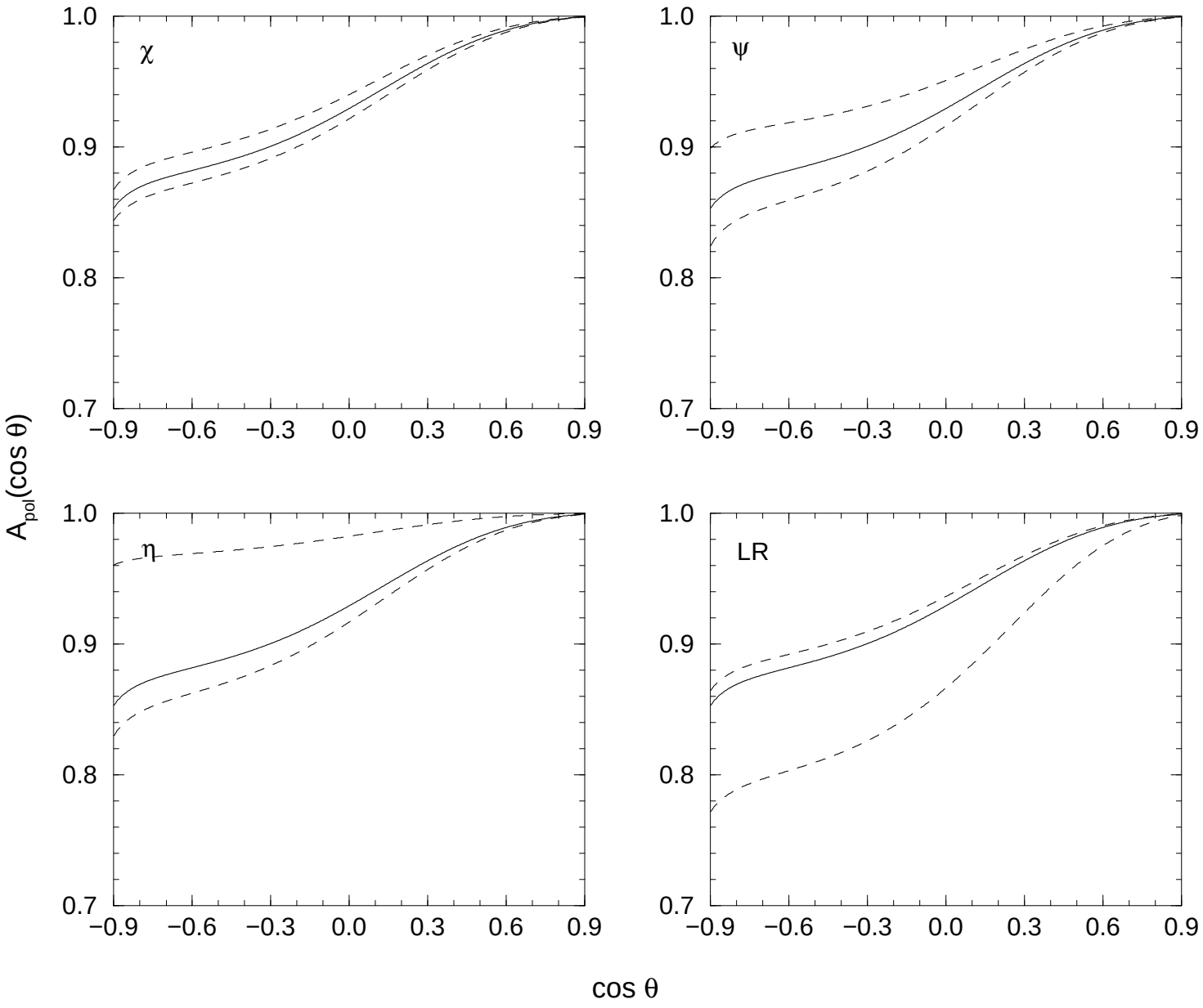

Fig. 8